

## Patch-based Land Cover Change Detection using Multitemporal and Multivariate Alteration Detection of Optical Satellite Imagery

Bo-Yi Lin (1), Chao-Hung Lin (1)

<sup>1</sup>Department of Geomatics, National Cheng-Kung University, Tainan, Taiwan

Email: [pikadp2004@hotmail.com](mailto:pikadp2004@hotmail.com); [linhung@mail.ncku.edu.tw](mailto:linhung@mail.ncku.edu.tw)

**KEY WORDS:** patch-based change detection, multitemporal and multivariate alteration detection, Generalized Canonical Correlation Analysis

**ABSTRACT:** Land-use/land-cover change detection is one of the most important applications of remote-sensing images. With the development of satellite and sensor techniques, the complexity of change detection caused by the improvement of image spatial resolution is increasing. The spatial unit of data analysis is generally altered from a pixel to a patch that contains not only spectral information but also local spatial and texture information. For change detection algorithms, previous studies focused on subtracting pixels/objects using a statistical approach called Multivariate Alteration Detection (MAD) from bitemporal images. However, the problem of inconsistency caused by dealing with more than two optical satellite images has not been addressed. This paper introduces a novel method, called Multitemporal Multivariate Alteration Detection (MMAD), to alleviate this problem. This method is based on weighted generalized canonical correlation analysis, which solves canonical coefficients for multivariable and multitemporal data, thereby resulting in consistent change detection. In addition, a new weighting scheme based on object similarity, image quality, and temporal coherence is introduced into MMAD to reduce the sensitivity to large landcover changes and to stably distinguish changed from non-changed area. Moreover, combining patch information with MMAD can improve the detection accuracy and make the proposed method feasible and obtain reasonable results.

### 1 Introduction

With the development of satellite and sensor techniques, many applications on remote sensing have arisen with a lot of attentions, such as land cover change detection, precision agriculture, and environment monitoring. In land cover change detection, changed information can be used for natural resource management, urban development, and natural disaster monitoring, as well as for predicting possible change patterns in the near future. Theoretically, changes on the Earth surface within a certain period can be detected through multitemporal remote-sensing images (Bao et al., 2012, Bruzzone and Prieto, 2000).

Different change detection techniques based on image algebra have been developed. One common approach, the application of a threshold value to differentiate change from non-change, is used in most of the change detection algorithms, which is simple and easy to interpret results. (Coppin and Bauer, 1996) utilized image differencing to detect changes in forest ecosystems. However, the decision of a suitable threshold value is a challenge, especially for those images without radiometric normalization or correction. Therefore, Howarth and Wickware (1981) proposed a method using image ratioing to detect environmental changes, which can handle the image calibration errors, including sun angle, shadow and topography impact (Rignot and vanZyl, 1993). Some approaches utilized the logistic regression to model the changes from forest to non-forest (Ludeke et al., 1990) and deforestation change measuring, which reduces the adverse effect by atmospheric conditions and sun angles (Singh, 1986).

Unlike the direct comparison, the approaches using transformation from images are famous.

The usage of the difference from vegetation index can reduce the impacts of topographic effects and illumination, but the random or coherence noise would be a problem (Nordberg and Evertson, 2005, Sohl, 1999, Wilson and Sader, 2002); change vector analysis (CVA) can process any number of spectral bands desired and produce detailed change detection information, however, encountered the difficulties in identifying land cover change trajectories and the requirement of the remote-sensing data acquired from the same phenological period (Chen et al., 2003). Then, a statistical approach called Principle component analysis (PCA) is used for the land-cover and land-use change detection, which reduces the redundancy of data and emphasizes different information in the derived components (Byrne et al., 1980).

Although PCA can provide high-quality change detection, it is applied to a spectral band of a multispectral image, which may result in inconsistent change detection among spectral bands. Therefore, Nielsen et al. (1998) proposed a statistical-based method, called Multivariate Alteration Detection (MAD), to find the main projected direction of the difference from bitemporal images to obtain the lowest correlation.

MAD is invariant to linear and affine scaling, which implies that linear atmospheric and sensor effects will not influence the change detection. However, MAD is unsuitable to deal with images that contain many significant changes because the calculation of covariance matrix in MAD is sensitive to outliers such as cloud pixels/patches. As a result, the method called iteratively reweighted MAD (IR-MAD) was introduced to address this problem (Canty and Nielsen, 2008, Nielsen, 2007). This method employs a weighted scheme to reduce the impact of outliers and the significant change of pixels/patches in the covariance matrix computation and to gradually distinguish unchanged pixels/patches from changed ones. However, normalization using IR-MAD still includes some challenging problems requiring solutions. First, a good initial weight should be provided for good convergence in the iteratively reweighting process. Second, numerous changed pixels/patches in bitemporal images may result in inappropriate projections of MAD variates in IR-MAD. For these reasons, Marpu et al. (2011) proposed the usage of initial change mask to eliminate significantly changed pixels/patches in bitemporal images before performing IR-MAD.

These related methods above solely deal with bitemporal images, and the problem of radiometric normalization for more than two images remained unaddressed. A novel method called multitemporal and multivariate alteration detection (MMAD) is proposed in the present study to overcome this challenge. The proposed method simultaneously deals with multitemporal and multispectral images to discriminate unchanged pixels/patches from changed ones in an image sequence, which leads to consistent change detection.

## **2 Related Work**

In this study, changes in multitemporal and multispectral satellite images are detected by the proposed MMAD, which is an extension of MAD (Nielsen et al., 1998). In this section, MAD technique and a statistical algorithm named Generalized Canonical Correlation Analysis, which can handle the calculation of the cross-correlation matrices of more than two random variables, are briefly reviewed in Section 2.1 and Section 2.2, respectively.

## 2.1 Review of MAD

The concept of MAD is to detect PIFs via canonical correlation analysis (CCA). CCA is a generalization of the Pearson correlation between two random variables  $\mathbf{X}$  and  $\mathbf{Y}$ . For optical satellite images, the canonical variables  $\mathbf{P}$  and  $\mathbf{Q}$  are defined as linear combinations of two multispectral images with  $b$  bands; that is,

$$\begin{cases} \mathbf{P} = \alpha_x^T \mathbf{X} = \alpha_{x1}X_1 + \alpha_{x2}X_2 + \dots + \alpha_{xb}X_b \\ \mathbf{Q} = \alpha_y^T \mathbf{Y} = \alpha_{y1}Y_1 + \alpha_{y2}Y_2 + \dots + \alpha_{yb}Y_b \end{cases}, \quad (1)$$

where  $\mathbf{X}$  and  $\mathbf{Y}$  represent the random vectors of the digital numbers of bitemporal images  $I_x$  and  $I_y$ , and  $\alpha_x$  and  $\alpha_y$  denote unknown coefficient vectors. Nielsen et al. (1998) proposed to solve unknown coefficients by minimizing the correlation between  $\mathbf{P}$  and  $\mathbf{Q}$ . That is, the variance of  $\mathbf{P} - \mathbf{Q}$ , which is denoted by  $Var(\mathbf{P} - \mathbf{Q})$ , is maximized under the constraints  $Var\{\alpha_x^T \mathbf{X}\} = Var\{\alpha_y^T \mathbf{Y}\} = 1$ . The optimization equation is written as

$$\begin{aligned} & \arg \max_{\alpha_x, \alpha_y} Var\{\alpha_x^T \mathbf{X} - \alpha_y^T \mathbf{Y}\} \\ & \text{subject to } Var\{\alpha_x^T \mathbf{X}\} = Var\{\alpha_y^T \mathbf{Y}\} = 1 \end{aligned} \quad (2)$$

After obtaining the coefficients  $\alpha_x$  and  $\alpha_y$ , the MAD components of the bitemporal images are derived using

$$\mathbf{MAD}_i = \mathbf{P}_i - \mathbf{Q}_i = \alpha_{xi}^T \mathbf{X} - \alpha_{yi}^T \mathbf{Y}, \quad i = 1 \cdots N, \quad (3)$$

where  $i$  represents the band index of the bitemporal images. The first MAD component has the minimum spread in the digital number of patches, which indicates that the first MAD component has the maximum amount. The second MAD component has the second maximum amount of unchanged information.

## 2.2 Review of Generalized CCA (GCCA)

GCCA is a statistical algorithm for calculating the cross-correlation matrices of more than two random variables by using multiblock data analysis and partial least squares (PLS) (Tenenhaus et al., 2015). The objective function of GCCA is similar to that of CCA. Eq.(2) for CCA is modified to deal with multiple random variables as follows:

$$\begin{aligned} & \max_{\alpha_1 \cdots \alpha_m} \sum_{i,j=1; i \neq j}^m C_{ij} \text{Cov}(\alpha_i^T \mathbf{X}_i, \alpha_j^T \mathbf{X}_j), \\ & \begin{cases} C_{ij} = 1, & \text{if } \mathbf{X}_i \text{ and } \mathbf{X}_j \text{ are connected} \\ C_{ij} = 0, & \text{otherwise} \end{cases} \\ & \text{subject to } Var\{\alpha_i^T \mathbf{X}_i\} = 1, \quad i = 1, \cdots, m, \end{aligned} \quad (4)$$

where  $\mathbf{X}_i$  and  $\mathbf{X}_j$  are random variables,  $\alpha_i$  and  $\alpha_j$  are their corresponding unknown coefficient vectors, and  $m$  represents the number of input images. Given a sequence of satellite images  $\{I_1, \cdots, I_m\}$ , a graph that represents the connection of input images is established. In this

graph, adjacent images are connected. In addition, the errors resulting from the optimization of  $\text{Cov}(\alpha_1^T \mathbf{X}_1, \alpha_2^T \mathbf{X}_2)$  may propagate toward the optimization of the next calculation in  $\text{Cov}(\alpha_{m-1}^T \mathbf{X}_{m-1}, \alpha_m^T \mathbf{X}_m)$ . Therefore, a connection is assigned to the first and last images to address the error propagation problem. Image connection is controlled by multiplier  $C$ . If images  $I_i$  and  $I_j$  are connected, then  $C_{ij}$  is set to 1. Otherwise,  $C_{ij}$  is set to 0.

Solving the constrained objective function in Eq.(4) with the aid of Lagrange multipliers yields the following stationary equations:

$$\Sigma_{ii}^{-1} \sum_{j=1; i \neq j}^m C_{ij} (\alpha_i^T \Sigma_{ij} \alpha_j) \Sigma_{ij} \alpha_j = \lambda_i \alpha_i, \quad (5)$$

where  $\{\lambda_1, \dots, \lambda_m\}$  are the Lagrange multipliers.  $\Sigma_{ii}$  represents the variance matrix of random vector  $\mathbf{X}_i$ , and  $\Sigma_{ij}$  denotes the cross-covariance matrix between  $\mathbf{X}_i$  and  $\mathbf{X}_j$ . In contrast with CCA, which obtains coefficient vectors by solving the coupled generalized eigenvalue problem, the optimization equation, i.e., in Eq.(5), does not provide an analytical solution for the coefficients  $\{\alpha_1, \dots, \alpha_m\}$ . Nevertheless, the stationary equations can be utilized to construct a monotonically convergent algorithm for the optimization problem. In particular, the coefficients  $\{\alpha_1, \dots, \alpha_m\}$  are derived using an iterative scheme. With the aid of inner component  $\mathbf{V}$ , which is introduced into the PLS algorithm, the stationary equation can be simplified and the difficulty in computing the coefficients  $\{\alpha_1, \dots, \alpha_m\}$  can be reduced. With the inner component, the equation is transformed to

$$\alpha_i = \frac{\Sigma_{ii}^{-1} \text{Cov}(\mathbf{X}_i, \mathbf{V}_i)}{[\text{Cov}(\mathbf{X}_i, \mathbf{V}_i)^T \Sigma_{ii}^{-1} \text{Cov}(\mathbf{X}_i, \mathbf{V}_i)]^{\frac{1}{2}}}, \quad i = 1, \dots, m, \quad (6)$$

where the covariance matrix  $\text{Cov}(\mathbf{X}_i, \mathbf{V}_i)$  between the random vector  $\mathbf{X}_i$  and its corresponding inner component  $\mathbf{V}_i$  is defined as

$$\text{Cov}(\mathbf{X}_i, \mathbf{V}_i) = \sum_{j=1; i \neq j}^m C_{ij} \Sigma_{ij} \alpha_j. \quad (7)$$

Through Eqs.(6) and (7), the unknown coefficients  $\{\alpha_1, \dots, \alpha_m\}$  can be derived through an iterative scheme using the PLS algorithm. The iterative process is formulated as

$$\alpha_i^{S+1} = \frac{\Sigma_{ii}^{-1} \text{Cov}(\mathbf{X}_i, \mathbf{V}_i^S)}{[\text{Cov}(\mathbf{X}_i, \mathbf{V}_i^S)^T \Sigma_{ii}^{-1} \text{Cov}(\mathbf{X}_i, \mathbf{V}_i^S)]^{\frac{1}{2}}}, \quad i = 1, \dots, m, \quad (8)$$





where  $S$  represents the iteration index, and  $\mathbf{V}_i$  denotes the inner component of image  $I_i$ . The unknown coefficients  $\{\alpha_1, \dots, \alpha_m\}$  are obtained when the iteration meets a termination criterion. A criterion is defined as follows: the differences between the current and previous iteration coefficients are less than a specified threshold.

### 3 Methodology

#### 3.1 Dataset and Study Area

Landsat 8 satellite, where the Operational Land Imager (OLI) and Thermal Infrared Sensor (TIRS) are instruments onboard, containing ten spectral bands and one panchromatic band. The spatial resolutions of the spectral and panchromatic bands are 30 m and 15 m, respectively. The Istanbul Airport was selected as the study area in this paper, and four different dates in same season from year 2013 to 2019 are employed with spectral information band 1 to band 7 of Landsat-8, as shown in Figure 1. To consider computational cost, image blocks of  $700 \times 700$  pixels were tested.

Table 1: Study area in Istanbul Airport from four different dates in same season.

True Color Image				
	Date 1	Date 2	Date 3	Date 4
Location (path, row)	(180, 31)			
Band usage	Band 1 to Band 7 (coastal to Short Wave Infrared)			
Acquisition Date	2013/07/30	2016/07/22	2017/07/25	2019/07/31

#### 3.2 Data Preprocessing

Patch-based change detection technology takes advantage in detecting group of like pixels together. In this paper, four images are used simultaneously in order to obtain the same patch pattern for all dates. Then, patch information are acquired using the software named eCognition applying multi-resolution segmentation and spectral difference segmentation to merge similar patches. Then, 729 image patches are generated with the information of mean digital number from band 1 to band 7 and texture information including the mean of GLCM Homogeneity, GLCM angular second moment, and GLCM entropy from all multispectral bands.

#### 3.3 Weighted Generalized Canonical Correlation Analysis

In the GCCA scheme, the unknown coefficients  $\{\alpha_1, \dots, \alpha_m\}$  in the objective function are simultaneously optimized using iterative processes. The WGCCA algorithm is proposed to solve the problem of erroneously distinguishing changed and unchanged patches. This algorithm is inspired by IR-MAD, which introduces a reweighting scheme to reduce the impact of patches with a considerable change and the outliers in covariance matrix calculation. The coefficients  $\{\alpha_1, \dots, \alpha_m\}$  in WGCCA are derived from an iterative reweighted scheme. With the reweighting scheme, the unchanged between the connected images are likely to be distinguished from the changed patches. In the beginning of the iteration, two components have to be initialized, namely, the unknown coefficients  $\{\alpha_1^0, \dots, \alpha_m^0\}$  and weights  $\{w_1^0, \dots, w_n^0\}$ , where  $n$  represents the number of patches in an image. An iteration process relies on good initial values, which can facilitate convergence and the search for global optimal coefficients. First, the initial values of coefficients  $\{\alpha_1^0, \dots, \alpha_m^0\}$  are obtained from the CCA of the connected image pairs. Each initial coefficient  $\alpha_i^0$  is set to the average of coefficient  $\alpha_{i(i-1,i)}^0$  from the CCA of the connected images  $(I_{i-1}, I_i)$

and coefficient  $\alpha_{i(i,i+1)}^0$  from that of another connected images ( $I_i, I_{i+1}$ ). Second, in contrast with IR-MAD, which sets an initial weight of one to all the patches, the proposed method sets a patch spectral angle in the connected images as the initial weight. The spectral angle of a patch in connected images is defined in Eq.(9), in which a patch pair with a small spectral angle and high spectral similarity is assigned a large weight. After the first iteration, the subsequent iteration adopts different weighting strategies from the initial weights. Two factors are considered, namely, normalized MAD (NMAD) and temporal coherence. Following the suggestion of Canty and Nielsen (2008), the NMAD obtained in the previous iteration is used as the patch weight. To enhance unchanged patches, the temporal coherence factor is defined as the difference between the digital numbers of a patch and the median digital numbers of the corresponding patches in the temporal domain. By combining the initial weight and the two reweighting scheme factors, the patch weight in the iterative process is defined as

$$\begin{cases} w_{ij}^k = N_1 \left\{ \cos^{-1} \left( \frac{\mathbf{p}_j^i \cdot \mathbf{p}_j^{i+1}}{\|\mathbf{p}_j^i\| \|\mathbf{p}_j^{i+1}\|} \right) \right\}, k = 0 \\ w_{ij}^k = \frac{1}{N_2(NMAD_i(j))} \times \frac{1}{N_3(TC_i(j))}, k = 1, \dots, n_{it}, \end{cases} \quad (9)$$

where  $k$  denotes the iteration index, and  $n_{it}$  represents the number of iterations. Patch  $\mathbf{p}_j$  in the connected images  $I_i$  and  $I_{i+1}$  is represented as  $\mathbf{p}_j^i$  and  $\mathbf{p}_j^{i+1}$ , respectively. The NMAD and temporal coherence values of patch  $\mathbf{p}_j$  in image  $I_i$  are denoted as  $NMAD_i(j)$  and  $TC_i(j)$ , respectively. Functions  $N_1(\cdot)$ ,  $N_2(\cdot)$ , and  $N_3(\cdot)$  are used to normalize the input quantities within the range of [0.0001, 1.0]. In GCCA, a covariance matrix is used to derive the unknown coefficients. By contrast, in WGCCA, a weighted covariance matrix, which is denoted as  $\tilde{\Sigma}$ , is used to solve the unknown coefficients in WGCCA. The weighted covariance matrix is defined as

$$\tilde{\Sigma}_{ii} = \frac{1}{n} \sum_{j=1}^n \frac{w_{ij}(X_{ij} - \bar{X}_i)(X_{ij} - \bar{X}_i)}{\sum_{j=1}^n w_{ij}}, \quad \bar{X} = \frac{\sum_{j=1}^n w_{ij}X_{ij}}{\sum_{j=1}^n w_{ij}}. \quad (10)$$

With the reweighting scheme, the covariance matrix  $Cov(\mathbf{X}_i, \mathbf{V}_i)$  in Eq.(6) is replaced with the weighted covariance matrix  $wCov(\mathbf{X}_i, \mathbf{V}_i)$ , and Eq.(6) is reformatted as

$$\alpha_i^{S+1} = \frac{\tilde{\Sigma}_{ii}^{-1} wCov(\mathbf{X}_i, \mathbf{V}_i^S)}{[wCov(\mathbf{X}_i, \mathbf{V}_i^S)^T \tilde{\Sigma}_{ii}^{-1} wCov(\mathbf{X}_i, \mathbf{V}_i^S)]^{\frac{1}{2}}}, \quad i = 1, \dots, m, \quad (11)$$

where  $wCov(\mathbf{X}_i, \mathbf{V}_i^S)$  represents the weighted covariance matrix of random variable  $\mathbf{X}_i$  and the corresponding inner component  $\mathbf{V}_i^S$  at the  $S^{th}$  iteration, which is defined as

$$wCov(\mathbf{X}_i, \mathbf{V}_i^S) = \sum_{i,j=1;i \neq j}^m C_{ij} \tilde{\Sigma}_{ij} \alpha_j^S. \quad (12)$$

The NMAD of the connected images are generated using the final coefficients  $\{\alpha_1^{S+1}, \dots, \alpha_m^{S+1}\}$ . The patch is likely to be classified as changed if the patch value of the NMAD image is high. By contrast, the patch can be considered as non-changed if the patch value of the NMAD

image is low. Thus, the value of the NMAD image can be regarded as a measure for distinguishing changed from non-changed patches. The entire WGCCA process is illustrated in Figure 1. First, a connected graph for the input image sequence is designed. Second, the iterative process starts with an initial value of the unknown coefficients  $\{\alpha_1^0, \dots, \alpha_m^0\}$  and patch weights  $\{w_1^0, \dots, w_n^0\}$ . During the iteration, the coefficients are updated using Eq.(11), and the patch weights are updated using Eq.(9). The process is terminated when the difference between the current and previous iteration coefficients is less than a specified threshold, i.e.,  $\sum_{i=1}^m |\alpha_i^{S+1} - \alpha_i^S| < \tau$ .

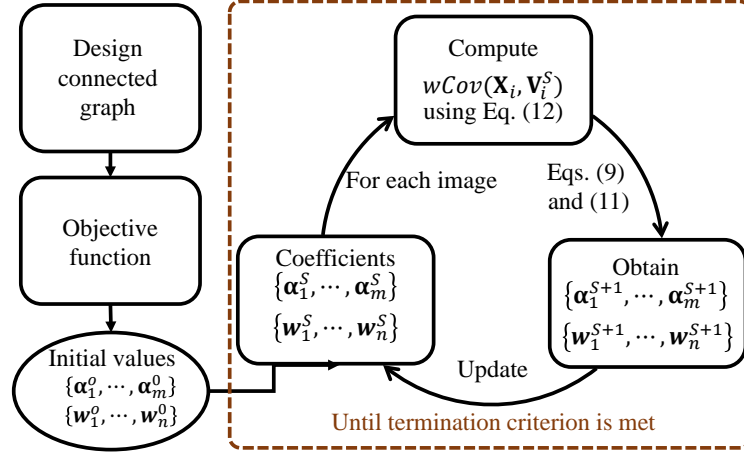


Figure 1: WGCCA workflow.

### 3.4 Change Detection

The NMAD image can be obtained for each connected image pair by using WGCCA. To further refine the NMAD of each image and further reduce misclassifications, particularly of cloud covers, the NMAD of the connected image pairs  $(I_i, I_{i+1})$  and  $(I_{i-1}, I_i)$  is combined with weights to form the NMAD of a single image at the middle of the connected images, i.e.,  $I_i$ . The correlation coefficient of the connected image pair is utilized as weight. If the correlation coefficient of the connected image pair is high, then a few changed patches exist in this image pair, and a high weight is assigned. In this manner, the NMAD of each image is determined by the linear combination of NMAD of the corresponding connected images, i.e.,

$$NMAD_i^* = \frac{\sum_{j=1; j \neq i}^m C_{ij} \times Coef_{ij} \times NMAD_{ij}}{\sum_{j=1; j \neq i}^m Coef_{ij}}, i = 1, \dots, m, \quad (13)$$

where  $NMAD_{ij}$  and  $Coef_{ij}$  represent the normalized MAD and correlation coefficient of connected images  $I_i$  and  $I_j$ , respectively.  $NMAD_i^*$  represents the combined NMAD for image  $I_i$ .

## 4 Experimental Results

### 4.1 Evaluation of change detection

Three change detection methods, namely, MAD (Canty et al., 2004), IR-MAD (Canty and Nielsen, 2008, Nielsen, 2007), and the proposed MMAD method, were compared using the dataset containing four images acquired on different days. The results of the NMAD image and the change detection map are presented in Figures 2. The NMAD image represents the possibility of change patches, which are depicted in blue to yellow corresponding to change possibility from low to high. For a fair comparison, the threshold for selecting unchanged patches from the NMAD image is the same. To visualize the results, unchanged patches are marked with true colors, whereas the others are displayed in red. In MAD and IR-MAD, NMAD images are generated from image pairs, whereas in MMAD, NMAD images are generated from all images. In particular, a set of unchanged patches is extracted simultaneously from all images in MMAD, therefore, the result of MMAD is no need to show in pairs. In MAD and IR-MAD, the change detection results are visually similar and over detected. However, for MMAD, which consider all temporal information at once, is more robust than the other two compared methods.

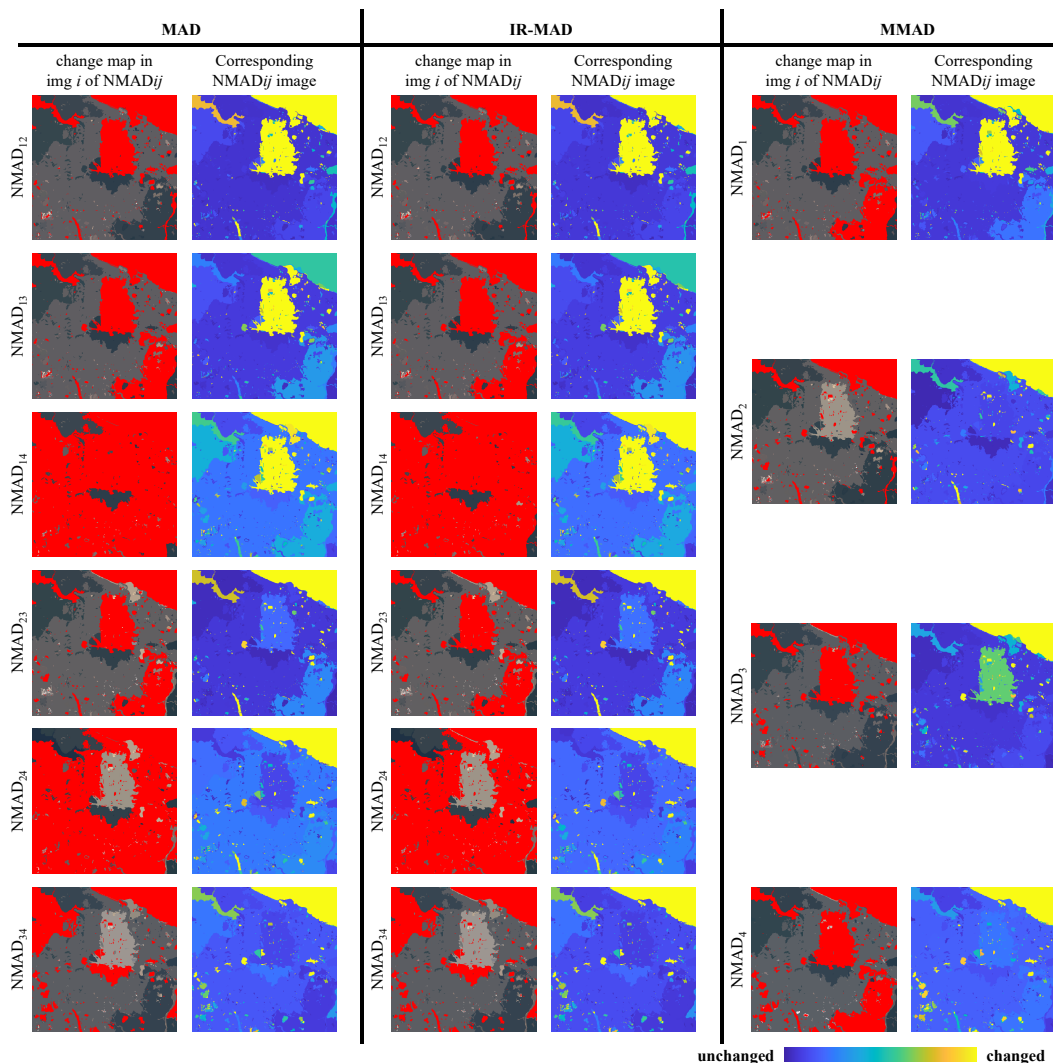


Figure 2: Comparison of change detection using MAD, IR-MAD, and the proposed MMAD. Changed and unchanged patches are displayed in red and true color, respectively; NMAD images are depicted from blue to yellow corresponding to change possibility from low to high.



## 4.2 Evaluation of texture features

The comparison of using texture information are presented in Figure 3, where three change detection methods, namely MAD, IR-MAD, and proposed MMAD, were compared. In this experiment, the performance of MMAD shows the highest stability in adding texture information. Besides, the change detection without texture information only consider the mean reflectance of the patches, which has lack details in the patch of the Istanbul airport undetected using the threshold defined by chi-square distribution. By contrast, the results with texture feature consider the information of the patch pattern and the airport is successfully detected as change patch.

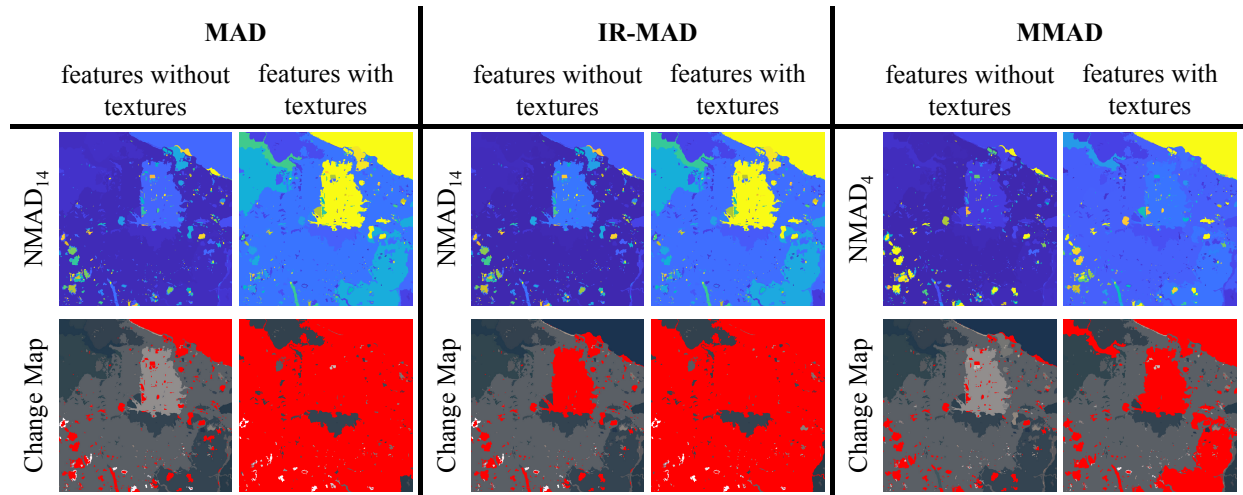


Figure 3: Comparison of using texture features between MAD, IR-MAD, and the proposed MMAD. 1<sup>st</sup> row: NMAD image of image pair in date 1 and 4 for MAD and IR-MAD, and NMAD image in date 4 for MMAD; 2<sup>nd</sup> row: change map for date 4.

## 5 Conclusions

A novel method called MMAD is proposed for detecting changed patches from a satellite image sequence instead of pairwise extracting those from bitemporal images. The proposed method is based on WGCCA which solves the canonical coefficients for multivariate and multitemporal data, thereby resulting in a consistent change detection. Two sets of SPOT-5 multitemporal images were tested in the experiments. From the visual comparison of the extracted changed patches, along with the quantitative analysis of the selected non-changed patches, we conclude that the results of the proposed MMAD are better than those of MAD and IR-MAD in terms of the quality of the selected non-changed patches, particularly for multitemporal images with considerable landcover changes. In this study, the weighting scheme based on patch similarity, image quality, and temporal coherence is introduced into MMAD to reduce the sensitivity of change detection to cloud covers and to stably distinguish changed from non-changed patches.

## References

Bao, N., Lechner, A. M., Fletcher, A., Mellor, A., Mulligan, D., Bai, Z., 2012. Comparison of relative radiometric normalization methods using pseudo-invariant features for change detection studies in rural and urban landscapes. *Journal of Applied Remote Sensing* 6 (1), 063578–1.

- Bruzzone, L., Prieto, D. F., 2000. Automatic analysis of the difference image for unsupervised change detection. *IEEE Transactions on Geoscience and Remote sensing* 38 (3), 1171–1182.
- Byrne, G. F., Crapper, P. F., Mayo, K. K., 1980. Monitoring land-cover change by principal component analysis of multitemporal landsat data. *Remote Sensing of Environment* 10, 175–184.
- Canty, M. J., Nielsen, A. A., 2008. Automatic radiometric normalization of multitemporal satellite imagery with the iteratively re-weighted MAD transformation. *Remote Sensing of Environment* 112 (3), 1025–1036.
- Canty, M. J., Nielsen, A. A., Schmidt, M., 2004. Automatic radiometric normalization of multitemporal satellite imagery. *Remote Sensing of Environment* 91 (3), 441–451.
- Chen, J., Gong, P., He, C., Pu, R., Shi, P., 2003. Land-use/land-cover change detection using improved change-vector analysis. *Photogrammetric Engineering and Remote Sensing* 69, 369–379.
- Coppin, P. R., Bauer, M. E., 1996. Digital change detection in forest ecosystems with remote sensing imagery. *Remote Sensing Reviews* 13, 207–234.
- Howarth, P. J., Wickware, G. M., 1981. Procedures for change detection using Landsat digital data. *International Journal of Remote Sensing* 2, 277–291.
- Ludeke, A. K., Maggio, R. C., Reid, L. M., 1990. An analysis of anthropogenic deforestation using logistic regression and GIS. *Journal of Environmental Management* 31, 247–259.
- Marpu, P. R., Gamba, P., Canty, M. J., 2011. Improving change detection results of IR-MAD by eliminating strong changes. *IEEE Geoscience and Remote Sensing Letters* 8 (4), 799–803.
- Nielsen, A. A., 2007. The regularized iteratively reweighted MAD method for change detection in multi-and hyperspectral data. *IEEE Transactions on Image processing* 16 (2), 463–478.
- Nielsen, A. A., Conradsen, K., Simpson, J. J., 1998. Multivariate alteration detection (MAD) and MAF postprocessing in multispectral, bitemporal image data: New approaches to change detection studies. *Remote Sensing of Environment* 64 (1), 1–19.
- Nordberg, M. L., Evertson, J., 2005. Vegetation index differencing and linear regression for change detection in a Swedish mountain range using Landsat TM® and ETM+® imagery. *Land Degradation and Development* 16, 139–149.
- Rignot, E. J. M., vanZyl, J. J., 1993. Change detection techniques for ERS-1 SAR data. *IEEE Transactions on Geoscience and Remote Sensing* 31, 896–906.
- Singh, A., 1986. Change detection in the tropical forest environment of northeastern India using Landsat. *Remote sensing and tropical land management*. J. Wiley, New York, 237–254.
- Sohl, T. L., 1999. Change analysis in the United Arab Emirates: an investigation of techniques. *Photogrammetric Engineering and Remote Sensing* 65, 475–484.
- Tenenhaus, A., Philippe, C., Frouin, V., 2015. Kernel generalized canonical correlation analysis. *Computational Statistics & Data Analysis* 90, 114–131.
- Wilson, E. H., Sader, S. A., 2002. Detection of forest harvest type using multiple dates of Landsat TM imagery. *Remote Sensing of Environment* 80, 385–396.